Scientific Reports

https://doi.org/10.1038/s41598-026-61574-8

Article in Press

COVLIAS 3.5: integration of attention-based segmentation technique with fuzzy dilated convolutional neural networks for improved classification of chest X-ray scans for multiclass pneumonia diagnosis

Received: 6 April 2026

Accepted: 6 July 2026

Published online: 21 July 2026

Cite this article as: Dubey A.K., Jain A., Vashist S. *et al.* COVLIAS 3.5: integration of attention-based segmentation technique with fuzzy dilated convolutional neural networks for improved classification of chest X-ray scans for multiclass pneumonia diagnosis. *Sci Rep* (2026). https://doi.org/10.1038/s41598-026-61574-8

Arun K. Dubey, Achin Jain, Shruti Vashist, Anurag Choubey, Kumar Shashvat, Luca Saba & Jasjit S. Suri

COVLIAS 3.5: Integration of Attention-based Segmentation Technique with Fuzzy Dilated Convolutional Neural Networks for Improved Classification of Chest X-ray Scans for Multiclass Pneumonia Diagnosis

Arun K. Dubey[1,3], Achin Jain[1,3], Shruti Vashist[2], Anurag Choubey[4], Kumar Shashvat[5,*], Luca Saba[6], and Jasjit S. Suri[7,8,9,10]

[1]Department of Information Technology, Bharati Vidyapeeth's College of Engineering, New Delhi 110063, India
[2]Department of ECE, Manav Rachna University, Sector-43, Aravali Hills, Surajkund Road, Faridabad, Haryana 121001, India
[3]Research Fellow, INTI International University, Persiaran Perdana BBN Putra Nilai, 71800 Nilai, Negeri Sembilan, Malaysia
[4]Department of Computer Science and Engineering, Technocrats Institute of Technology, Bhopal 462022, India
[5]Department of Computer Science and Engineering, Manipal University Jaipur, India
[6]Department of Radiology, Azienda Ospedaliero Universitaria (A.O.U.) di Cagliari, Cagliari, Italy
[7]Stroke Diagnostic and Monitoring Division, AtheroPoint, Roseville, CA, USA
[8]Department of Electrical and Computer Engineering, Idaho State University, Pocatello, ID, USA
[9]Global Biomedical Technologies, Inc., Roseville, CA, USA
[10]Symbiosis Institute of Technology, Nagpur Campus, Symbiosis International (Deemed University), Pune, India
[*]Corresponding author: Kumar Shashvat (e-mail: kumar.shashvat@jaipur.manipal.edu)

March 2026

Abstract

This study aims to improve pneumonia diagnosis by integrating attention-based U-Net models for lung segmentation with fuzzy logic-enhanced CNNs for classification. This approach addresses the limitations of inadequate modelling of complex spatial relationships in medical images. The underutilization of fuzzy logic with dilated convolutions has restricted the extraction of multiscale features. We utilized 18,608 chest X-ray (CXR) images. Subsequently, these images were segmented using four models namely: U-Net, Attention U-Net, Pruned U-Net and U-Net++. Fuzzy logic system was used to process the segmented data. Additionally, we show that the dilated CNN architecture for improved classification performance. In lung segmentation, our experimental results indicate that Attention U-Net (AU) achieved 1% better mean accuracy, 2% better mean Jaccard and Dice than U-Net, pruned U-Net and U-Net++. In the classification, the model has demonstrated 10% better mean accuracy over augmented U-Net and Attention U-Net based segmented data. ROCs have shown that augmented effect has 15% better AUC in bacterial pneumonia class. Additionally, we saw a 4% improvement with fuzzy logic. The integration of fuzzy dilated CNN with Attention U-Net segmentation presents a 1% better accuracy compared to U-Net. Best AUC achieved was 0.98 in bacterial pneumonia. Our findings underscore the critical role of attention mechanisms and augmentation in enhancing medical image analysis. The integration of Attention U-Net for segmentation and fuzzy dilated CNN for multi-class classification significantly improves diagnostic accuracy and reliability. This approach has the potential to revolutionize pneumonia diagnosis, leading to better patient outcomes and more efficient healthcare delivery.

Keywords: Chest X-ray; pneumonia; lung segmentation; attention; fuzzy logic; dilated CNN.

1 Introduction

Medical image analysis of chest X-ray interpretation plays a pivotal role in diagnosing respiratory diseases [1]. Coronavirus Disease (COVID), viral pneumonia, bacterial pneumonia, and tuberculosis are closely related lung disease [2–4]. Deep learning (DL) is preferred over machine learning (ML) for pneumonia prediction [5]. This is due to better performance outcomes and automatic feature extraction [6–8] for viral pneumonia [9, 10] and bacterial pneumonia [11] are different due to virus and bacterial effects.

In the realm of respiratory diseases, the differentiation between conditions like bacterial pneumonia, viral pneumonia, COVID-19, and tuberculosis remains a significant challenge, compounded by the high mortality rates, substantial healthcare costs, and complex co-morbidities associated with these illnesses [12–17]. The current diagnostic paradigm, based on the interpretation of traditional radiographs has limitations in reliability and accuracy that require advanced solutions [18]. The urgency of this research is highlighted by the dual burdens posed on the health and economic system worldwide, as well as the complexities those respiratory diseases such COVID-19, pneumonia and tuberculosis bring in term of co-morbidity. This places a substantial financial burden on global health systems through associated direct costs for treatment and indirect impacts upon productivity, whilst facing healthcare providers with myriad challenges in patient management which fundamentally arise from the systemic interplay of these diseases. Our effort is aimed at tackling these profound issues by proposing an advanced DL-based diagnostic tool that will improve the accuracy and efficiency of diagnosis to significantly reduce economic burden, while maintaining standard patient care in case of multiple co-morbidities [19–21].

A single-center cohort study assessed [22] pneumonia in 585 mechanically ventilated patients, including 190 with COVID-19, with ICU physicians adjudicating episodes. CarpeDiem, a machine-learning tool, revealed prolonged ICU stays among COVID-19 [23] patients due to respiratory failure, with higher mortality rates associated with unresolved ventilator-associated pneumonia (VAP). A multicentre, double-blind, randomized, controlled, superiority trial provides compelling evidence supporting the efficacy and safety of inhaled amikacin as a therapeutic intervention in critically ill adults undergoing invasive mechanical ventilation [24, 25].

Segmentation helps medical images to extract relevant section for the classification of disease [26–29]. For lung image segmentation [30], we explore four distinct architectures: U-Net [31], Pruned U-Net [32], Attention U-Net [33], and U-Net++ [34]. These models are specifically tailored for medical image segmentation, leveraging their ability to capture spatial information and generate precise segmentation masks [35]. U-Net, a convolutional neural network (CNN) based encoder-decoder architecture, serves as the baseline model [5, 36, 37]. Basic architecture of our model (COVLIAS 3.5) is depicted in Figure 1. It is divided into three parts: segmentation, preprocessing using fuzzy logic and classification model.

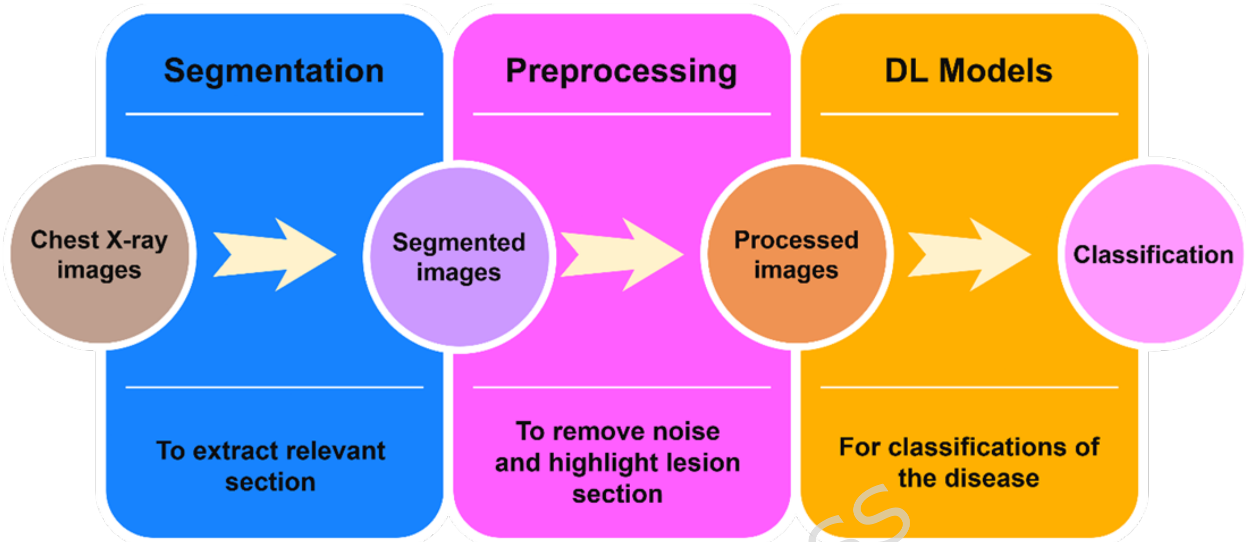

Figure 1: COVLIAS 3.5: Basic architecture of medical image analysis. DL: Deep Learning.

Throughout our experiments, we evaluate the performance of each model using a range of evaluation metrics, including the Jaccard index [38], Dice coefficient [39], accuracy, recall, area under the curve (AUC), precision, and F1-score. These metrics provide valuable insights into the efficacy of our proposed methodologies in accurately segmenting abnormalities and classifying chest X-ray images. At the core of our study lies the supposition that utilizing state-of-the-art segmentation architectures and FDCNN for classification will give remarkable results concerning accurately pinpointing respiratory diseases as opposed to traditional models. This hypothesis provides the basis for our experimental design and metric selection, which serve as a representation of how we are dedicated to pushing the limits on medical imaging. We also explore how different augmentation techniques can improve the performance of our model, hence leading to a more robust and generalizing AI-model [40, 41]. In a novel approach to the field of medical image segmentation and classification, this study seeks to apply fuzzy logic with dilated CNNs. Additionally, the sophistication of advanced data augmentation strategies to enhance model generalization and performance promise a significant advancement that goes beyond current state-of-the-art approaches in applying DL for medical diagnostics. The validation of our hypotheses in this study remains outside the scope and scale required for accepted use but will be significant at application levels as it can solve a major unmet clinical need;

This paper is structured into eight sections. The first section provides an introduction, followed by the background in the second section. The third section details the materials and methods used. The fourth section presents the experimental results, and the fifth section discusses the ROC analysis of the classification model. The sixth section addresses the reliability and stability of the AI models. In the seventh section, we provide a discussion of the findings. Lastly, the final section offers the conclusion.

2. Background Literature

Recent events have underscored the critical limitations inherent in conventional diagnostic methodologies when confronting pulmonary diseases. These shortcomings have been particularly apparent in the diagnosis and management of conditions such as tuberculosis, viral pneumonia, bacterial pneumonia, and most notably, throughout the unprecedented challenges of the COVID-19 pandemic. This backdrop highlights an urgent need for the advancement and adoption of more effective diagnostic techniques to better address and mitigate the impact of lung disorders [42]. Despite being essential for the clinical evaluation of these illnesses, chest CT scans and X-rays have several intrinsic drawbacks, including high expense, restricted accessibility, and subjective interpretation [43–47]. These difficulties not only jeopardize the accuracy of diagnoses but also highlight how urgent it is for medical imaging technologies to progress.

The use of AI in medical imaging has had a transformational impact (source) on the discipline and presents exciting opportunities to address long-term challenges. Early uses of AI, particularly methods with machine learning, made a strong case for reshaping diagnoses. One major development was the emergence of DL and CNNs [48–52]. CNNs have been broadly utilized in recognizing CXRs and CT images because of their capacity for progressive element extraction, demonstrating better execution to recognize strong and weak signalization lung diseases [53, 54]. Artificial intelligence has led to new developments in medical imaging, with machine learning algorithms promising early advancements for improving diagnostics [55–58]. A remarkable step was introduced with the evolution of DL, more specifically CNNs which outperform for CXR and CT images analysis due to high level feature extraction. Thus, enhancing detection and classification of lung diseases. In recent years fuzzy logic has been explored in AI models which served as an advanced guide to image assessment [59, 60]. Fuzzy logic can be very useful in image analysis of pulmonary diseases as it is able to interpret contradiction and uncertainties which may lead a more robust and accurate diagnosis.

Jiang et al. [61] has explained the importance of fuzzy in medical imaging but utilization of larger receptive field is missing. Similarly Narayan et al. [62] explained the use of FuzzyNet for effective classification of medical image dataset but utilization oof fuzzy for feature vector is missing. Zhao et al. [63] and Wang et al. [64] have helped us to utilize the attention mechanisms with fuzzy network to get better features for classification. In this paper, we seek to address this gap by integrating advanced segmentation techniques using classification using fuzzy logic-enhanced CNNs [65] to improve the diagnostic accuracy and reliability of pneumonia detection in chest X-rays.

Given the complexity and variability in lung diseases, particularly in multi-class classification scenarios [66], we hypothesize that integrating fuzzy logic into the classification framework can be highly effective. This study, therefore, introduces a new dimension to the research in this field, emphasizing the potential of fuzzy logic to enhance classification accuracy and robustness. The limited number of studies exploring this approach underscores the novelty and significance of our investigation, pushing the boundaries of current research and offering substantial contributions to the field of medical imaging.

3. Materials and Method

In this work, we have extracted the features from different state-of-the-art techniques to improve chest X-ray image analysis. It helps us to propose a novel methodology with pre-processed fuzzy data. The complete methodology is divided into four sections. First 18608 X-ray images are collected and pre-processed for training, validation, and testing. In the second step, we segmented the data using four segmentation models U-Net, U-Net++, Pruned U-Net, and Attention U-Net. The best outcome among the four has been utilized for the third step, fuzzy logic, we have used fuzzy logic to deal with uncertainty and imprecision in the image dataset. This processed clean data is utilized for classification using Dilated CNN models. This helps us to utilize a larger receptive field for multiclass classification. The experiments conducted in the study compare these segmentation models, using FDCNN and augmenting techniques. The performance of the models has been assessed using evaluation metrics such as accuracy, recall, precision, F1-score, Dice, and Jaccard to ensure robustness against clinically relevant outcomes.

3.1 Data Collection and Preprocessing

We used 18,608 chest X-ray images extracted from three different datasets: the "COVID-19 Radiography Dataset," the "Chest X-ray Images (Pneumonia)" dataset and finally, the 'Tuberculosis' TB Chest X-Ray Database. Covid-19 Radiography Dataset (3,616 COVID-19 images + 1,345 VP Images + 10,167 Normal Images). We selected all COVID-19, VP, and normal images from this dataset. The "Chest X-ray Images (Pneumonia)" data was provided by the Guangzhou Women and Children's Medical Centre, and contains 5,863 X-rays, including 2,780 bacterial pneumonia (BP) images, all of which we used. The "Tuberculosis (TB) Chest X-ray Database" includes 700 images of TB patients, and we utilized all these TB images. To validate the model, we randomly selected 10% of the images for validation and another 10% for testing from each class, ensuring each class was equally represented. To balance the class of the dataset, we have also performed augmentation [67] after fuzzy preprocessing data [68].

Dataset assembly and baseline curation follow the approach of Nillmani et al. [87]. Authors have assembled the COVID-19 Radiography Database, Chest X-ray Images (Pneumonia), and Tuberculosis Chest X-ray Database for multiclass pneumonia classification.

3.2 Four Image Segmentation models: U-Net, Pruned U-Net, Attention U-Net, U-Net++

U-Net Architecture

It is CNN based encoder-decoder architecture. It is well-suited for segmenting images of our medical images. The U-Net's ability to capture spatial information and generate accurate segmentations helped us to segment desired section. It can effectively learn features from the input images and produce corresponding segmentation masks, providing valuable insights into the regions of interest within the images. Our U-Net model is presented in Figure2

Pruned U-Net

Given the relatively smaller size of our dataset images, employing a Pruned U-Net can help optimize computational resources without compromising segmentation performance [32]. Pruned U-Net can remove unnecessary parameters and build a more effective model to the target features given. This make sure that the segmentation tasks can be achieved easily on devices with considerably lower computational capabilities.

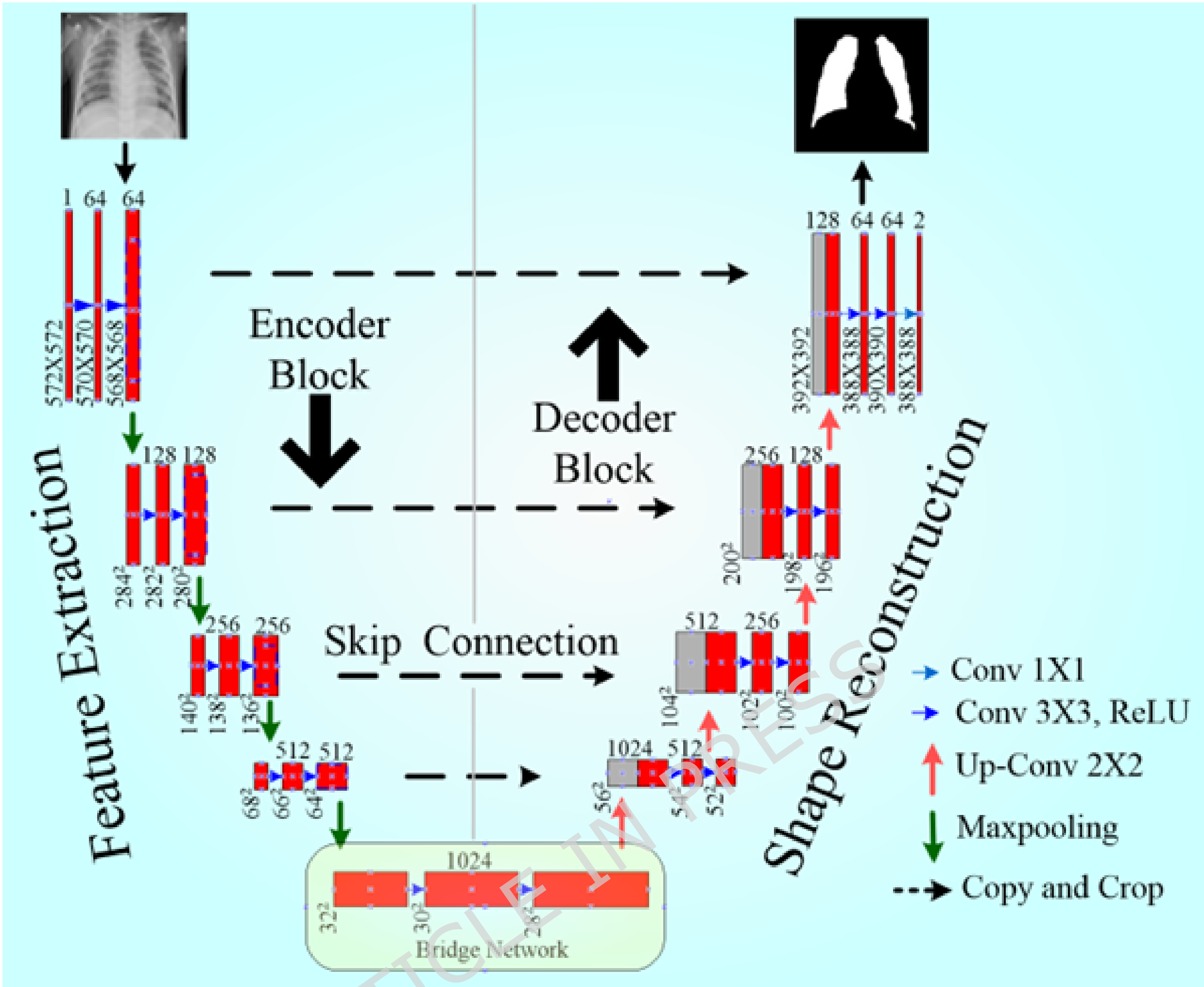

Figure 2: U-Net architecture for segmentation.

Attention U-Net

Attention U-Net would be useful in this dataset as it allows the network to focus on a particular region, when necessary, thus improving the accuracy of the segmentation. In the dataset, only the lungs, heart, and clavicles are to be segmented, which means that it can be useful to focus on the details and ensure no other anatomical features are labelled. In other words, unlike the organ focusing, attention U-Net can be used to make sure no noise is introduced in the segmentation.

U-Net++

U-Net++ is derived from the fundamental U-Net structure as an attempt to overcome its deficiency in effective hierarchical feature capturing by the encoder. This technique takes advantage of skip connections at the different levels through the encoder and the decoder [69]. The intent is to capture multiscale information and enhance the capability to obtain higher-level features that can refine the previous point of the object position at an alternative stage. U-Net++ can not only improve the accuracy of image segmentation but also increase the robustness of the technique in relation to items of various shapes and sizes. U-Net, Selected U-Net, Attention U-Net, and U-Net++ haves are the four main segments in the process used for segmentation [35]. The process is applied to extract a specific portion. The attribute is also classified after being processed over fuzzy logic.

3.2 Fuzzy-Based Dilated CNN Architecture

We have proposed an architectural framework wherein original images and their corresponding masks traverse through a series of segmentation models U-Net, Pruned U-Net, Attention U-Net, and U-Net++. These segmentation models are meticulously designed to effectively delineate the intricate features present within the images. The resultant predicted masks serve as pivotal components in the segmentation process, facilitating the accurate categorization of images into five distinct classes: Covid, Normal, Tuberculosis, Viral Pneumonia, and Bacterial Pneumonia.

To pre-process the segmented images, we use fuzzy logic that deals with uncertainty and imprecision. It helps us with noise reduction and image enhancement of segmented images. Fuzzy logic is a better method for handling uncertainty in images by choosing an intermediate value between true and false. We have used four steps for this process. In the first fuzzy logic process, we converted the pixel intensities saved into a variable. We defined it as dark (Dark (I(x, y))) medium (Medium(I(x, y))) and bright (Bright(I(x, y))). After this, we have used fuzzy rules to increase, leave or decrease the brightness of pixels. Fuzzy rules are utilized for fuzzy inferences. It helps to evaluate the antecedent of each rule using fuzzy logic operators (AND, OR, and NOT). It also computes the degree of truth for each rule. The last process of defuzzification has been performed. It converts the fuzzy output into a crispy output by aggregating the fuzzy inferences results.

Let I represent the input pixel intensity, and O represent the output brightness adjustment. The fuzzy sets D, M, and B represent the membership functions for dark, medium, and bright pixel intensities respectively. Then, the fuzzy rules can be represented as:

- If I is D, then O Increases.
- If I is M, then O should Leave.
- If I is B, then O Decreases.

Mathematically, these rules can be represented as a set of if-then rules:

- If I is D(i), then O is Increases (o) with membership function μ increases (o).
- If I is M(i), then O is Leave(o) with membership function μ Leave(o).
- If I is B(i), then O is Decrease(o) with membership function μ Decrease(o).

These membership functions μIncrease(o), μLeave(o), and μDecrease(o) determine the degree to which the brightness should be increased, left unchanged, or decreased based on the intensity of the pixel. After pre-processing the images, we used dilated CNN for classification. It captures the larger contextual information compared to traditional CNN. It also adds gaps in the convolution kernels and allows sparser feature learning. Dilated CNN can be performed with equation 1. To compute a dilated CNN operation, let's assume feature map X, filter W, output feature map Y, and dilation rate d.

$$Y[i,j] = \sum_{m,n} X[i \cdot s + m \cdot d, j \cdot s + n \cdot d] \times W[m,n] \tag{1}$$

Where, i and j represent the spatial indices of the output feature map, m and n are the spatial indices of the filter, s is the stride and d represents the dilation rate. Leveraging the K5 cross-validation protocol, the proposed architecture, Figure3, is adept at capturing and learning intricate patterns and relationships within the data. It depicts the overall architecture of CNN classification architecture. Figure4 illustrates the COVLIAS 3.5 system, a comprehensive AI pipeline for multiclass classification of lung conditions using medical images. The process begins with raw input images undergoing quality control procedures, including normalization and augmentation. Various segmentation models (U-Net, U-Net++, Attention U-Net, Pruned U-Net) are then employed to segment the lung regions, resulting in a segmented image. This segmented image is processed using fuzzy logic to enhance the decision-making process before being classified into specific conditions (Bacterial Pneumonia, COVID-19, Normal, Tuberculosis, Viral Pneumonia) by the AI model.

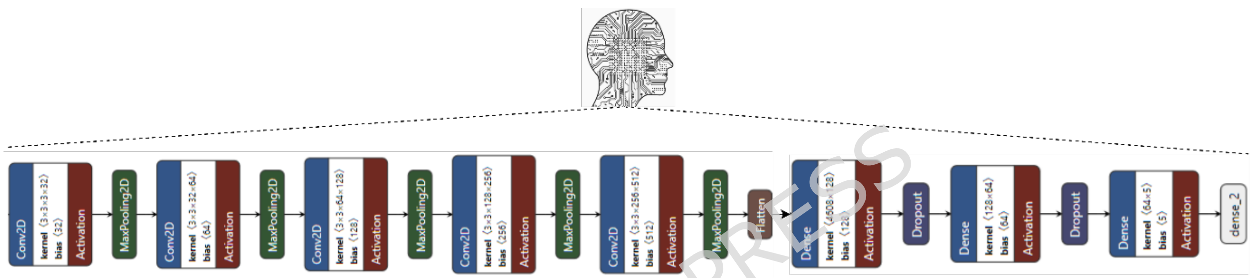

Figure 3: Overall architecture of AI model: CNN architecture.

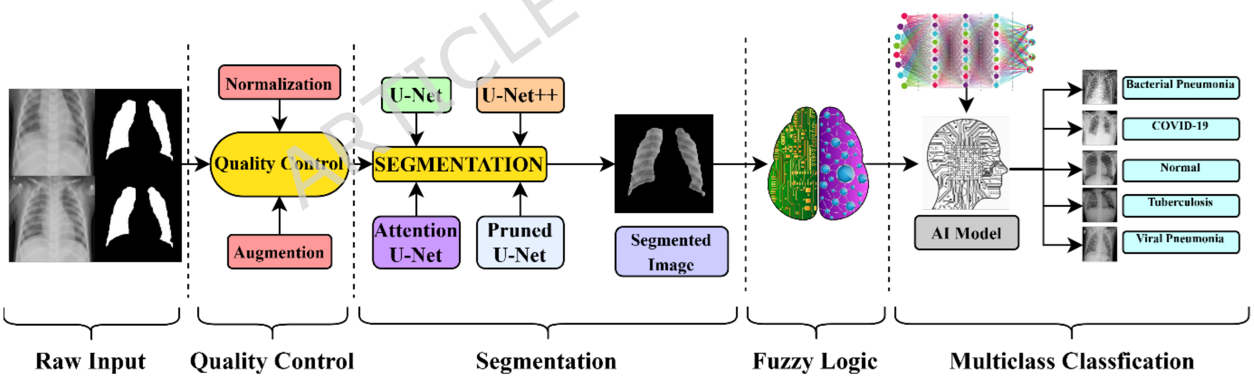

Figure 4: COVLIAS 3.5: Overall architecture of proposed AI system using FDCNN.

3.3 Experimental Protocols

Experiment 1: Comparing U-Net, Attention U-Net, Pruned U-Net, and U-Net++ for Segmentation

In this experiment, we compared the segmentation performance of four different models: U-Net, Attention U-Net, Pruned U-Net, and U-Net++. Each model was tasked with segmenting chest X-ray images to isolate regions indicative of various conditions, such as COVID, Normal, Tuberculosis, Viral Pneumonia, and Bacterial Pneumonia. We evaluated these models based on their ability to accurately capture relevant features within the images using metrics such as the Jaccard index, Dice coefficient, and overall segmentation accuracy. This experiment aimed to identify the most effective segmentation architecture for subsequent classification tasks.

Experiment 2: Implementing the Fuzzy Dilated CNN Method for Classification using Segmented Data

In the second experiment, we implemented a FDCNN method to classify the segmented images obtained from Experiment 1. The fuzzy logic component was used to pre-process the segmented images, enhancing their quality by reducing noise and handling uncertainty. The dilated CNN architecture then utilized these pre-processed images to classify them into five categories: COVID, Normal, Tuberculosis, Viral Pneumonia, and Bacterial Pneumonia. The performance of this classification model was assessed using precision, recall, F1-score, and the area-the-under-the-curve (AUC) to determine its effectiveness in accurately diagnosing the various conditions.

Experiment 3: Integrating Augmentation Techniques into the Training Pipeline

The third experiment focused on enhancing the model's robustness and generalizability by integrating data augmentation techniques into the training pipeline. This process involved artificially increasing the size and diversity of the training dataset through various transformations, such as rotations, translations, and scaling. By training the FDCNN on this augmented data, we aimed to improve its ability to generalize across different variations and achieve higher classification accuracy. The impact of data augmentation was measured by comparing the classification metrics, including precision, recall, F1-score, and AUC, before and after augmentation.

3.4 Evaluation Metrics

We employed metrics such as True Positive (TP), True Negative (TN), False Positive (FP), and False Negative (FN) to evaluate the performance of our models. These metrics facilitated the calculation of accuracy (η) as outlined in Equation 2, recall (ρ) in Equation 3, precision ($\wp$) in Equation 4, and F1-score ($\digamma$) in Equation 5. In addition, we used Dice and Jaccard coefficients, detailed in Equation 6 and Equation 7 respectively, where ζ denotes the intended target items and γ denotes the items identified by our model. Moreover, the ROC curve and the AUC were analysed to determine the models' ability to differentiate between classes effectively.

$$\eta = \frac{TP + TN}{TP + FP + FN + TN} \tag{2}$$

$$\rho = \frac{TP}{TP + FN} \tag{3}$$

$$\wp = \frac{TP}{TP + FN} \tag{4}$$

$$\digamma = 2 \cdot \frac{\wp \cdot \rho}{\wp + \rho} \tag{5}$$

$$\beta(\gamma,\zeta) = 2\frac{|\gamma||\zeta|}{|\gamma|+|\zeta|} \tag{6}$$

$$I(\gamma,\zeta) = \frac{\beta(\gamma,\zeta)}{2-\beta(\gamma,\zeta)} \tag{7}$$

3.5 Loss Function and Optimization

Categorical cross-entropy loss (Equation 8) is crucial for fine-tuning models, especially with imbalanced healthcare data. It penalizes incorrect predictions, thus encouraging accurate and reliable classifications. For tasks like identifying diabetes risk levels, it ensures sensitivity to less frequent, high-risk cases, improving predictive accuracy. In this study, we implemented cross-entropy loss to enhance model performance and clinical relevance, aiding early detection and stratification of diabetes risk, ultimately aiming to improve patient outcomes and healthcare efficiency.

$$\text{Categorical Cross-Entropy} = -\sum_{c=1}^{K} y_c \log(p_c) \tag{8}$$

In the Equation 8, K represents the total number of classes. Here, y_c is a binary indicator that takes the value 1 if the class c is the correct classification for the given observation and 0 otherwise. p_c denotes the predicted probability that the observation belongs to class c. This loss function measures the dissimilarity between the true class distribution and the predicted probability distribution, ensuring that the model's predictions become more aligned with the actual distribution of classes.

4. Experimental Results

In this section, we present the experimental results of our segmentation and classification models on medical imaging datasets. We evaluate the performance of various U-Net architectures, including U-Net, Pruned U-Net, Attention U-Net, and U-Net++, using metrics such as Jaccard, Dice, and accuracy. Additionally, we assess the classification performance of a FDCNN applied to segmented data, both with and without data augmentation, across multiple disease classes. The results underscore the importance of model architecture and optimization techniques in enhancing segmentation and classification accuracy, particularly in critical medical applications.

4.1 Segmentation Results

We have used U-Net, Pruned U-Net, Attention U-Net and U-Net++ for segmentation. Jaccard, Dice and accuracy for each class.

Bacterial Pneumonia

The Table 1 presents the performance metrics of four segmentation models in diagnosing Bacterial Pneumonia. Each model's accuracy, Jaccard index, and Dice coefficient are evaluated to gauge their effectiveness in accurately delineating the regions of interest. Among the models assessed, the U-Net architecture achieves an accuracy of 90.53%, with corresponding Jaccard and Dice scores of 88%

and 93.61%, respectively. The pruned version of U-Net maintains competitive performance, registering a slightly lower accuracy of 90.35% but achieving marginally better Jaccard and Dice scores at 88.23% and 93.7%, respectively. Notably, the Attention U-Net model demonstrates superior performance, attaining an accuracy of 90.73% along with impressive Jaccard and Dice scores of 89.05% and 94.21%, respectively. Conversely, U-Net++ exhibits a comparable accuracy of 90.31% to its counterparts but slightly lower Jaccard and Dice scores at 88% and 93.01%, respectively. These results underscore the significance of model architecture and optimization techniques in enhancing the accuracy and precision of segmentation tasks, particularly in critical medical applications like pneumonia diagnosis. Figure5 shows the predicted mask using these four models.

Table 1: Segmentation model performance matrix for all five classes.

Model	**Accuracy (%)**	**Jaccard (%)**	**Dice (%)**
Bacterial Pneumonia			
U-Net	90.53	88.00	93.61
Pruned U-Net	90.35	88.23	93.70
Attention U-Net	90.73	89.05	94.21
U-Net++	90.31	88.00	93.01

Tuberculosis

The U-Net architecture achieves a commendable accuracy of 90.59%, with corresponding Jaccard and Dice scores of 93.038% and 96.39%, respectively. Similarly, the pruned version of U-Net maintains high performance, recording a slightly higher accuracy of 90.72% while maintaining identical Jaccard and Dice scores at 93.04% and 96.39%, respectively. The Attention U-Net model emerges as the top performer in this context, boasting an accuracy of 90.85% along with impressive Jaccard and Dice scores of 93.33% and 96.55%, respectively. Contrastingly, U-Net++, although achieving a competitive accuracy of 90.26%, exhibits lower Jaccard and Dice scores at 87.98% and 93.36%, respectively. These results underscore the significance of model architecture and optimization techniques in improving the precision and efficacy of Tuberculosis detection through image segmentation, thereby potentially aiding in early diagnosis and treatment planning for this infectious disease.

COVID

As for the U-Net COVID dataset, it shows an efficient performance and reaches 93.83% accuracy with Jaccard and Dice as 95.57% and 97.73%. The pruned U-Net kept the same level of accuracy, with a reduction to 93.75% but very high Jaccard and Dice values as well, reaching 94.99% and 97.43%, respectively (Figures 4). This means that, in this setting a model compete for the best areas in the Attention U-Net emerges as our leading algorithm with an accuracy of 93.9%, along with incredible Jaccard and Dice scores reaching 96.37% and 98.15%, respectively. Nevertheless, with 92.12%, U-Net++ achieves a quite high accuracy although the Jaccard and Dice scores are much lower at 83.33% and 90.91%. These findings suggest a significant role for choosing appropriate model architectures and optimization strategies in the accurate segmentation of COVID-19-related abnormalities, which can contribute toward early diagnosis and treatment planning support to patients suffering from this disease.

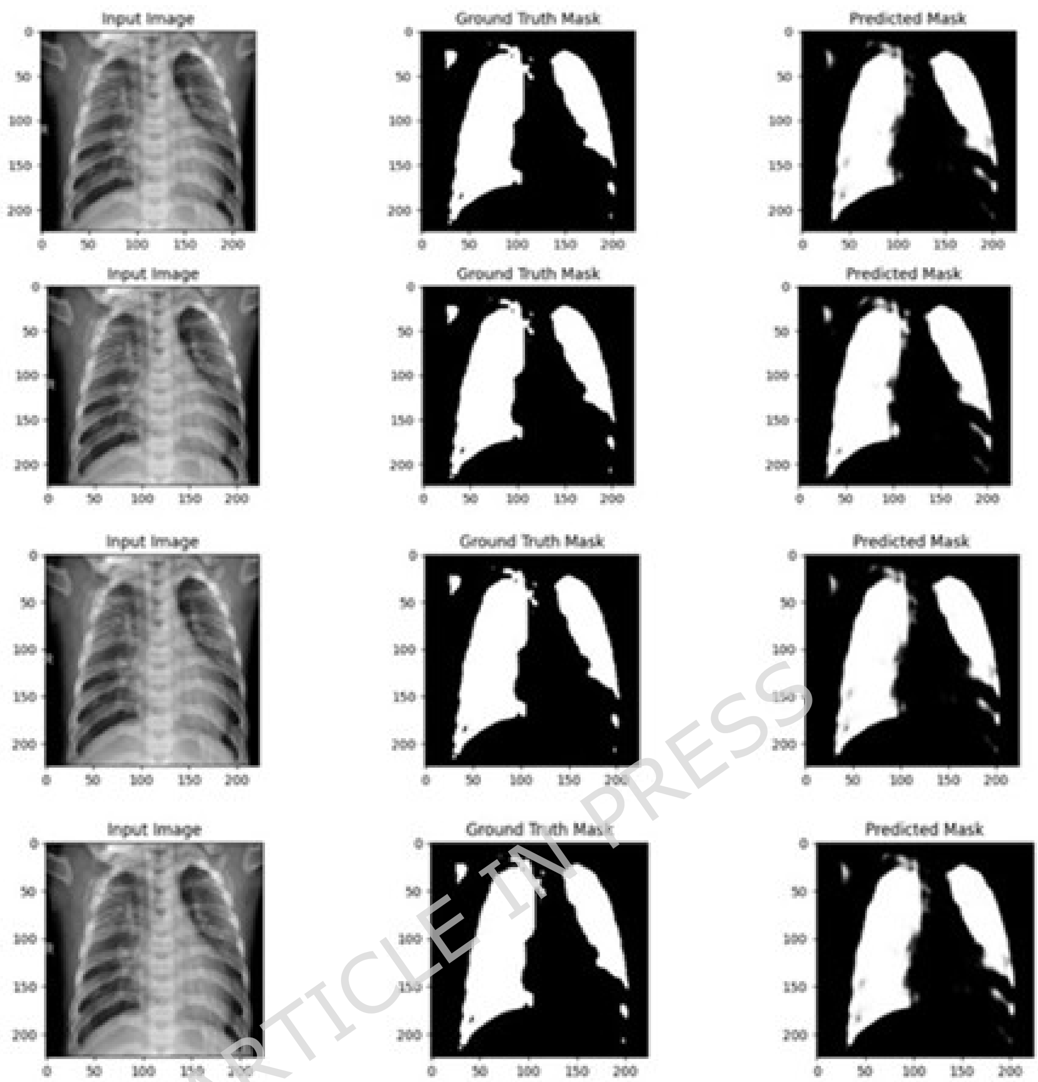

Figure 5: Row1: BP predicted mask using U-Net; Row2: BP predicted mask using Pruned U-Net; Row3: BP predicted mask using Attention U-Net; Row4: BP predicted mask using U-Net++.

Viral Pneumonia

The U-Net architecture shows excellent performance with an accuracy of 92.84% and Jaccard and Dice score at 94.62 and 97.24% respectively. Pruned U-Net shows a slightly reduced accuracy to 92.76% while producing impressive Jaccard and Dice scores of 94.09% and 96.95% respectively. Throughout all the experiments, we got an accuracy of 92.78% with Jaccard and Dice as 94.2% and 97.01%, which is competitive with the best models from Kaggle competition Attention U-Net model [12]. On the other side, U-Net++ which has good accuracy: 92.21% produces lesser Jaccard and Dice scores of 87.06% and 93.08%, respectively as such results highlight the importance of model architectures selection and optimization strategies for robust detection Viral Pneumonia-related abnormalities, to potentially assist in early diagnosis and treatment planning among patients with this condition.

Normal

U-Net architecture has successful performance with an accuracy of 98.63% and Jaccard score: 94.84%, Dice score: 97.35%. Figure 5: The pruned U-Net score an accuracy of 98.5%, competitive Jaccard and Dice scores equivalent to 94.84% and 97.35%, respectively. The Attention U-Net model outperforms with an accuracy of 98.69% and Jaccard score of 95.11%, Dice score - 97.49%. On the other hand, U-Net++ scores quite lower Jaccard and Dice values of 94.23% and 97.05%, despite its accuracy was relatively high at the level of 95.76%. This supports the selection of appropriate model architectures and optimization techniques in recognising normal regions from medial image data. Besides, normal tissue segmentation is a critical prerequisite for multiple medical applications like anomaly detection or disease diagnosis.

4.2 Classification Results

Results of multiclass classification using Fuzzy Dilated CNN

Table 2 illustrates the performance metrics of the Fuzzy Dilated CNN when applied to classify data segmented by U-Net without augmentation for several disease classes including Bacterial Pneumonia, COVID, Normal, Tuberculosis, and Viral Pneumonia. For Bacterial Pneumonia, the metrics show a precision of 0.81, a recall of 0.77, an F1-score of 0.79, and an AUC of 0.87, leading to an average accuracy of 84%. In COVID classifications, the precision reaches 0.81, recall stands at 0.75, F1-score at 0.78, and AUC at 0.85. The average accuracy detail is omitted. The model performs best with the Normal category, achieving a precision of 0.90, a recall of 0.95, an F1-score of 0.92, and an AUC of 0.91. The precision for Tuberculosis is 0.84 with a recall of 0.65, an F1-score of 0.74, and an AUC of 0.82. Viral Pneumonia classification shows lower results, with a precision of 0.55, a recall of 0.56, an F1-score of 0.55, and an AUC of 0.76.

Fuzzy dilated CNN over U-Net Segmented Data without and with Augmentation

According to Table2 when using augmented U-Net segmented data for classifying various conditions such as Bacterial Pneumonia, COVID, Normal, Tuberculosis, and Viral Pneumonia, the model's metrics vary. For Bacterial Pneumonia, it reports an impressive average accuracy of 94%, with precision at 0.89, recall at 0.91, an F1-score of 0.90, and an AUC of 0.95. For COVID, the precision is 0.93, recall is 0.90, F1-score is 0.92, and AUC is 0.94, though the average accuracy is not specified. The Normal category shows the highest accuracy at 97.02% as seen in the confusion matrix in Figure6, with precision at 0.96, recall at 0.98, F1-score at 0.97, and an AUC at 0.96. Tuberculosis classification is robust, showing a precision of 0.95, recall of 0.92, an F1-score of 0.94, and an AUC of 0.96. For Viral Pneumonia, the metrics are somewhat lower, with a precision of 0.82, recall of 0.78, F1-score of 0.80, and an AUC of 0.88.

Attention U-Net Segmented Data without and with Augmentation

The provided Table 3 outlines the evaluation metrics for the Attention U-Net segmented data using the Fuzzy Dilated CNN for classification without augmentation across various classes: Bacterial Pneumonia, COVID, Normal, Tuberculosis, and Viral Pneumonia. Each class is assessed based on precision, recall, F1-score, AUC, and mean accuracy. Bacterial Pneumonia: The Attention U-Net model achieves a precision of 0.87, recall of 0.84, F1-score of 0.85, and AUC of 0.91 for Bacterial

Table 2: Augmentation effect for classification model over U-Net segmented data.

Without Augmentation					
Pneumonia/Control Class	**Precision**	**Recall**	**F1-Score**	**AUC**	**Mean ACC (%)**
Bacterial Pneumonia	0.81	0.77	0.79	0.87	84
COVID	0.81	0.75	0.78	0.85	
Normal	0.90	0.95	0.92	0.91	
Tuberculosis	0.84	0.65	0.74	0.82	
Viral Pneumonia	0.55	0.56	0.55	0.76	
With Augmentation					
Bacterial Pneumonia	0.89	0.91	0.90	0.95	94
COVID	0.93	0.90	0.92	0.94	
Normal	0.96	0.98	0.97	0.96	
Tuberculosis	0.95	0.92	0.94	0.96	
Viral Pneumonia	0.82	0.78	0.80	0.88	

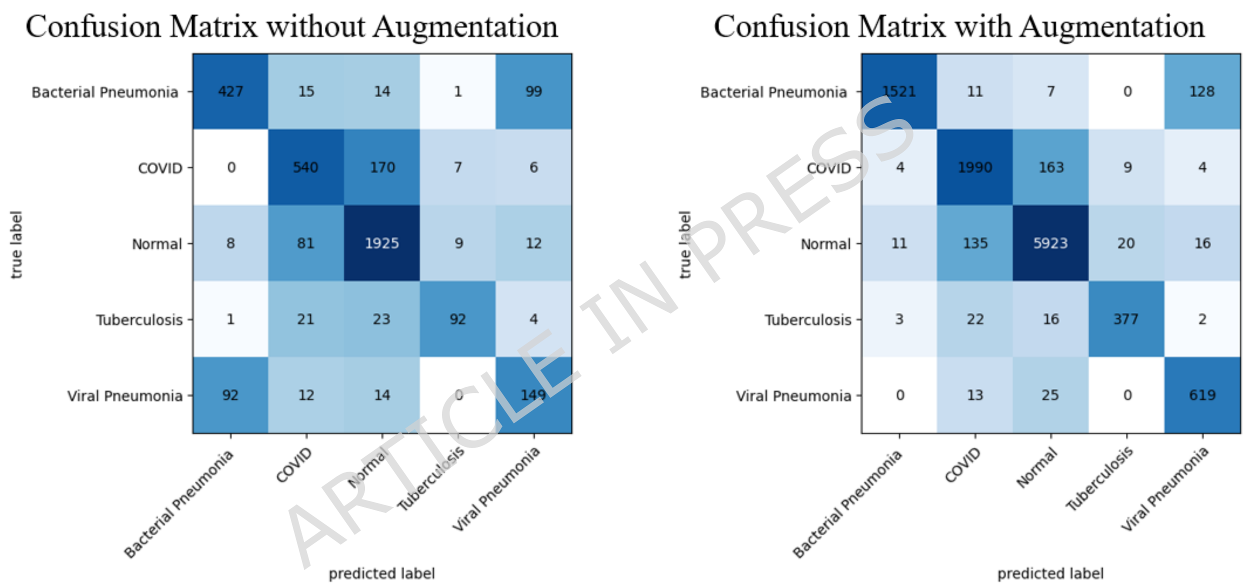

Figure 6: Confusion matrix without and with augmentation using U-Net

Pneumonia classification, with a mean accuracy of 85%. COVID: For COVID classification, the model demonstrates a precision of 0.8, recall of 0.72, F1-score of 0.76, and AUC of 0.84. The mean accuracy for COVID classification is not provided. Normal: In the case of Normal class classification, the model exhibits a precision of 0.88 and recall of 0.94, resulting in a balanced F1-score of 0.91 and AUC of 0.9. Tuberculosis: The model shows moderate performance in Tuberculosis classification, achieving a precision of 0.82, recall of 0.65, F1-score of 0.73, and AUC of 0.82. Viral Pneumonia: Lastly, for Viral Pneumonia classification, the model's precision, recall, and F1-score are relatively lower, with values of 0.7, 0.65, and 0.68, respectively. The AUC is reported as 0.81. These metrics provide insights into the performance of the Attention U-Net model across different classes. While the model demonstrates strong performance for some classes like Bacterial Pneumonia and Normal, there may be room for improvement, particularly in distinguishing Tuberculosis and Viral Pneumonia cases.

Attention U-Net Segmented Data with and without Augmentation

The Table 3 presents the evaluation metrics for the Fuzzy Dilated CNN model applied to classify Attention U-Net segmented data with augmentation across different classes: Bacterial Pneumonia, COVID, Normal, Tuberculosis, and Viral Pneumonia. Each class is evaluated based on precision, recall, F1-score, AUC, and mean accuracy. The model achieves outstanding precision: 0.92, recall: 0.98, F1-score: 0.95, and AUC: 0.98 for Bacterial Pneumonia classification, with a mean accuracy of 95% for Bacterial Pneumonia With augmentation. COVID: For COVID classification, the model demonstrates high precision: 0.91, recall: 0.94, F1-score: 0.93, and AUC: 0.96. The mean accuracy for COVID classification is not provided. Normal: In the case of Normal class classification, the model exhibits excellent precision of 0.98 and recall of 0.97, resulting in a balanced F1-score of 0.97 and AUC of 0.97. Tuberculosis: The model shows strong performance in Tuberculosis classification, achieving a precision: 0.97, recall: 0.89, F1-score: 0.93, and AUC: 0.95. Viral Pneumonia: Lastly, for Viral Pneumonia classification, the model's precision, recall, and F1-score are relatively high, with values of 0.94, 0.81, and 0.87, respectively. The AUC is reported as 0.9. Figure 7 also demonstrates the confusion matrix. It shows that BP class achieved highest accuracy 97.91% with augmentation. Performance metrics indicate the enhanced performance of the Fuzzy Dilated CNN model with augmentation across all five classes applying Attention U-Net segmented data. Augmentation techniques have effectively improved the model's power to generalize and classify between different classes, resulting in higher precision, recall, F1-scores, and AUC values. The mean accuracy also reflects the overall improvement in classification accuracy across all classes when augmentation is employed.

Table 3: Augmentation effect for classification model over Attention U-Net Segmented data.

Without Augmentation					
Pneumonia/Control Class	**Precision**	**Recall**	**F1-Score**	**AUC**	**Mean ACC (%)**
Bacterial Pneumonia	0.87	0.84	0.85	0.91	85
COVID	0.80	0.72	0.76	0.84	
Normal	0.88	0.94	0.91	0.90	
Tuberculosis	0.82	0.65	0.73	0.82	
Viral Pneumonia	0.70	0.65	0.68	0.81	
With Augmentation					
Bacterial Pneumonia	0.92	0.98	0.95	0.98	95
COVID	0.91	0.94	0.93	0.96	
Normal	0.98	0.97	0.97	0.97	
Tuberculosis	0.97	0.89	0.93	0.95	
Viral Pneumonia	0.94	0.81	0.87	0.90	

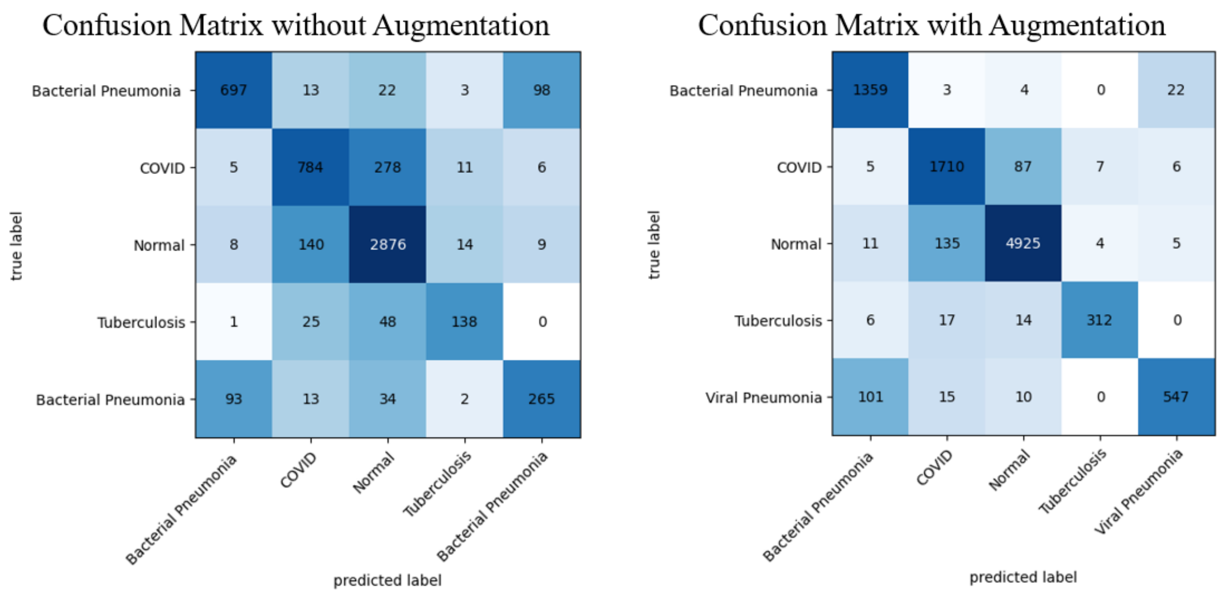

Figure 7: Confusion matrix without and with augmentation using Attention U-Net

5. Performance Evaluation

The Receiver Operating Characteristic (ROC) curve is a fundamental tool in assessing the performance of classification models, particularly in the context of medical image analysis. It plots the true positive rate (sensitivity) against the false positive rate (1-specificity) across various threshold values, providing a comprehensive visualization of a model's ability to discriminate between different classes. Each point on the ROC curve represents a sensitivity and specificity pair corresponding to a particular threshold setting. As the threshold changes, the true positive rate and false positive rate vary, thereby tracing out the ROC curve. A model with perfect discrimination would have an ROC curve that passes through the top-left corner of the plot, indicating high sensitivity and specificity across all threshold values. The AUC values for each class reflect the discriminatory power of the fuzzy dilated CNN model in distinguishing between positive and negative instances within the respective categories. A higher AUC signifies superior performance in classification.

U-Net without Augmentation

Here are the ROC results for Attention-U-Net segmented without augmentation, where p ¡ 0.001, Bacterial Pneumonia: The AUC of 0.87 indicates that the model has a strong ability to differentiate between instances of bacterial pneumonia and non-bacterial pneumonia. COVID: With an AUC of 0.85, the model demonstrates good discrimination between COVID-related abnormalities and normal cases. Normal: The AUC of 0.91 suggests excellent performance in identifying normal regions within medical images. Tuberculosis: Although slightly lower at 0.82, the AUC still indicates reasonable discrimination between tuberculosis cases and non-tuberculosis cases. Viral Pneumonia: With an AUC of 0.76, the model exhibits moderate performance in distinguishing viral pneumonia from other conditions. These AUC values provide valuable insights into the discriminatory ability of the fuzzy dilated CNN model across different classes, aiding in the evaluation and comparison of its performance in medical image classification tasks. Figure 8 shows ROC of Fuzzy Dilated CNN model for without augmentation U-Net Data.

U-Net segmented with Augmentation

The ROC results for Attention U-Net segmented with augmentation, where p ¡ 0.001, Bacterial Pneumonia: The model achieves an AUC of 0.95 for bacterial pneumonia classification, indicating strong discriminatory power in distinguishing between bacterial pneumonia and non-bacterial pneumonia cases. COVID: With an AUC of 0.94, the model demonstrates robust discrimination between COVID-related abnormalities and other conditions. Normal: The AUC of 0.96 reflects the model's high accuracy in identifying normal regions within medical images, showcasing excellent discriminatory power. Tuberculosis: Similarly, with an AUC of 0.96, the model exhibits strong discriminatory performance in distinguishing tuberculosis cases from non-tuberculosis cases. Viral Pneumonia: Although slightly lower at 0.88, the AUC still indicates moderate discrimination between viral pneumonia cases and other conditions. Figure 9 shows the ROC of Fuzzy Dilated CNN model for with augmentation U-Net Data.

Attention-U-Net segmented without augmentation

Next the ROC for Attention-U-Net segmented without augmentation results, where p ¡ 0.001 were as following, Bacterial Pneumonia: AUC=0.91, COVID: AUC=0.84, Normal: AUC=0.9, Tuberculosis: AUC=0.82, Viral Pneumonia: AUC=0.81. These results indicate the discriminatory ability of the model in distinguishing between different classes. Higher AUC values suggest better overall performance in classifying the respective conditions. The significance of p¡0.001 indicates that the observed AUC values are statistically significant, reinforcing the reliability of the model's performance. Figure 7c presents the ROC of Fuzzy Dilated CNN model for without augmentation Attention U-Net Data.

Attention-U-Net segmented with Augmentation

Attention U-Net segmented data with augmentation showed ROC results with p¡0.001 were quite impressive: Bacterial Pneumonia: AUC = 0.98, COVID: AUC = 0.96, Normal: AUC = 0.97, Tuberculosis: AUC = 0.95, Viral Pneumonia: AUC = 0.9. Figure 7d demonstrates ROC of the FDCNN model with augmentation with Attention U-Net segmented data.

Fuzzy Effect on the Model

The integration of Fuzzy Logic with Attention U-Net and U-Net has led to notable improvements in model performance across various conditions. This enhancement is highlighted by the increases in AUC values, as detailed in Table 4 and illustrated in Figure9. Specifically, the greatest improvement was observed in Covid detection, with an 8.51% increase, while the smallest was in Viral Pneumonia, at 3.41%. Furthermore, the application of augmented-based Attention U-Net with Fuzzy Logic to bacterial pneumonia detection achieved an AUC of 0.98, showcasing strong performance in the ROC analysis. This demonstrates the model's enhanced ability to accurately differentiate between different health conditions.

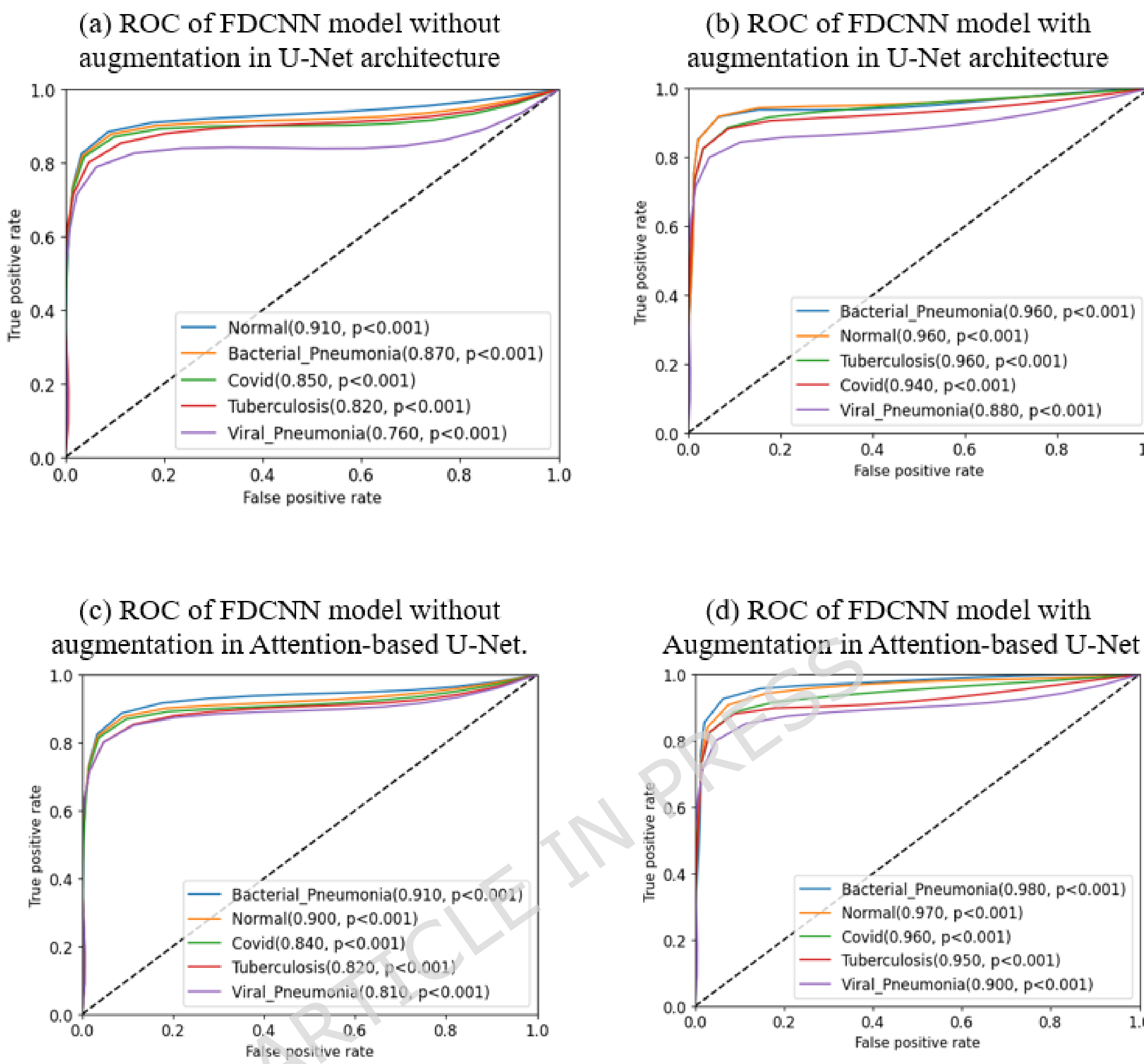

Figure 8: Comparison of ROC for FDCNN model based on Augmentation

Table 4: Comparison of Percentage Improvement (%) between U-Net with Fuzzy Logic and Attention U-Net with Fuzzy Logic

Class	U-Net with Fuzzy (%)	Attention U-Net with Fuzzy (%)
Bacterial Pneumonia	4.17	4.08
Normal	5.21	4.12
Tuberculosis	8.33	3.13
Covid	8.51	4.21
Viral_Pneumonia	3.41	3.33

6. Reliability and Stability of Fuzzy dilated CNN model

We have performed the Chi-Square test (CST) and Mann-Whitney test (MWT) to check system reliability. With a p-value less than 0.001, we reject the null hypothesis. This indicates strong evi-

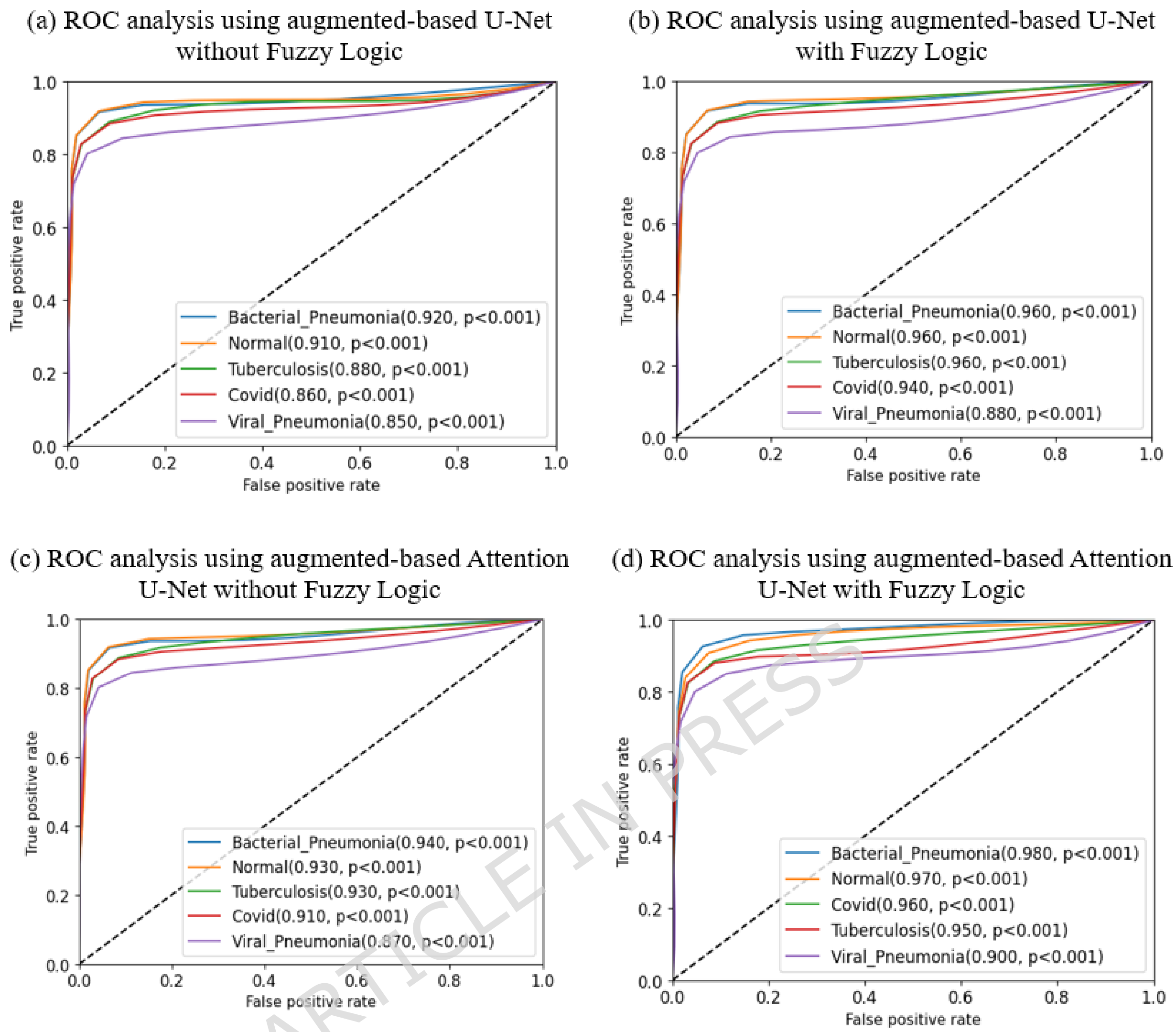

Figure 9: Comparison of ROC for FDCNN model based on fuzzy logic

dence that there is indeed a significant association between the Fuzzy + Dilated CNN methodology and the outcome variable. In the context of the MWT, it again suggested that there is a significant difference between the distributions of predictions for the tested COVID class and the other classes combined. Table 5 shows these two test results.

7. Discussion

The innovative integration of advanced segmentation techniques using U-Net, Pruned U-Net, Attention U-Net, and U-Net++ with the application of fuzzy logic for preprocessing, followed by classification through a dilated CNN, (i) represents a significant leap in the field of medical imaging for pulmonary diseases. (ii) This methodological synergy enhances the accuracy of segmenting complex medical images, where each U-Net variant contributes uniquely—U-Net provides a robust

Table 5: Statistical test analysis. Chi Square Test (CST) and Mann Witney Test (MWT).

With (w/) or Without (w/o) Augmentation	Methodology	CST (p-value)	MWT (p-value)
Proposed w/ and w/o Augmentation	Fuzzy+Dilated CNN	¡0.001	¡0.001
Proposed w/o Augmentation	Fuzzy+Dilated CNN	¡0.001	¡0.001
Proposed w/ Augmentation	Fuzzy+Dilated CNN	¡0.001	¡0.001

foundation, Pruned U-Net optimizes for computational efficiency, (iii) Attention U-Net focuses on salient regions enhancing detail recognition, and U-Net++ captures multi-scale information for refined analysis. (iv) Fuzzy logic plays a crucial role in noise reduction and image clarity enhancement, preparing images for more accurate classification by the dilated CNN. (v) This model's ability to handle subtle variations in disease presentation by effectively distinguishing between different types of pneumonia, tuberculosis, and COVID-19 related abnormalities underscores its potential to significantly improve diagnostic accuracy and reliability. (vi) By leveraging these advanced computational techniques, the proposed model not only addresses current challenges in pulmonary imaging but also sets a new standard for the application of AI in diagnosing complex respiratory diseases, offering profound implications for patient care and treatment planning.

Benchmarking

We have compared our proposed model with existing published models. These models have used CXR data or/and CT data. Keidar et al. [70] used an ensemble model featuring ResNet34/50/152 and VGG16 architectures, achieving and accuracy of 90.3% using CXR data. Peng et al. [71] utilized a model for CT and CXR data, achieving an accuracy of 84.3%. Wang et al. [72] employed a Support Vector Machine (SVM) on CT data, achieving an accuracy of 76.75%. Abdulah et al. [73] utilized an Attention paradigm combined with CNN model on private data, achieving an accuracy of 79%. Ayan et al. [74] employed an ensemble model on public data, achieving the highest accuracy of 95.83%. Additionally, the proposed model, without augmentation, incorporating Fuzzy combined with Dilated CNN architecture with U-Net segmentation achieved an accuracy of 84.43%, while with Attention U-Net segmentation; it achieved an accuracy of 85.44%. With augmentation, the proposed model attained higher accuracies of 93.25% and 95.07% for U-Net and Attention U-Net segmentation, respectively. Moreover, the proposed models demonstrated statistical significance with p-values ¡ 0.001. These findings offer valuable insights into the comparative performance of different segmentation methodologies in medical imaging applications. In this benchmarking, we achieved 5%, 10.77%, 18.2%, and 16.07% better accuracy in compare to Keidar et al. [70], Peng et al. [71], Yong Wang et al. [72] and Abdulah et al. [73], respectively. Table 6 depicts 12.5% better mean accuracy with augmentation in compared to an existing model.

A special note on the proposed model

Integrating U-Net, Pruned U-Net, together with our innovative Attention U-Net and U-net++ model, it shows that the proposed architecture has a significant improvement in terms of medical images segmentation over conventional methods. The effect of the attention mechanisms in U-Net architectures helps to concentrate on important characteristics resulting in highly improved segmentation accuracy. This precision is essential to appropriately recognize markers of disease that might be much more subtle.

Additionally fuzzy logic added in pre-processing makes our approach more adaptable and refined, improving the quality of segmented images which are then utilized for classification. Used in tandem with augmentation techniques for training, the FDCNN model performs favorably across various imaging states and shows strong robustness. The model has good repeatability and correlation, which may help with its clinical application according to the results of statistical analysis. A combination of advanced technology with state-of-the-art methodologies used in this comprehensive process, redefine medical imaging analysis output.

Table 6: Comparison of the proposed model with existing models.

Citation	**Methodology**	**Seg***	**Dataset**	**#S**	**#C**	**ACCU (%)**	**Mean AUC**	**p-value**
Keidar et al. [70]	Ensemble (ResNet/VGG)	Yes	CXR	1384	2	90.3%	0.96	No
Peng et al. [71]	Deep Learning model	No	CT+CXR	1590	3	84.3%	0.85	No
Wang et al. [72]	SVM	No	CT	244	3	76.75%	0.86	No
Abdulah et al. [73]	Attention+CNN	No	Private	3797	2	79%	0.85	No
Ayan et al. [74]	Ensemble	No	CXR	5856	2	95.83%	0.96	No
Proposed w/o Aug.	Fuzzy+Dilated CNN	U-Net	Private	18603	5	84.43%	0.91	¡0.001
Proposed w/o Aug.	Fuzzy+Dilated CNN	Att. U-Net	Private	18603	5	85.44%	0.94	¡0.001
Proposed w/ Aug.	Fuzzy+Dilated CNN	U-Net	Private	18603	5	93.25%	0.96	¡0.001
Proposed w/ Aug.	Fuzzy+Dilated CNN	Att. U-Net	Private	18603	5	95.07%	0.98	¡0.001

A special note on fuzzy logic

The integration of a fuzzy logic system prior to classification is motivated by its ability to handle uncertainty and imprecision present in medical images. In complex imaging tasks, such as those involving chest X-rays, features may not be distinctly defined, leading to difficulties in classification accuracy. Fuzzy logic can provide a framework for modelling this ambiguity, allowing for more nuanced decision-making that enhances feature extraction during segmentation, ultimately resulting in improved classification outcomes.The authors in [75–77] have demonstrated the effect of Fuzzy logic over COVID, Pneumonia X-ray dataset. The references build a strong hypothesis for the use of fuzzy logic by illustrating its applicability in similar domains, showcasing improvements in accuracy and reliability when integrated with machine learning techniques.

Fuzzy logic is introduced between segmentation and classification to refine the segmented regions and enhance the accuracy of the subsequent classification. By processing the segmented data through a fuzzy logic system, the nuances and uncertainties in the data can be better captured and interpreted, leading to more precise classification results. The fuzzy logic system typically accepts pre-processed data that has been segmented and possibly normalized. This data can include a range of values representing different degrees of membership in fuzzy sets, rather than crisp, binary values. This allows the system to handle data that is not strictly binary, capturing the inherent uncertainties and variability's present in medical images.

There are some drawbacks to the fuzzy logic system. Fuzzy logic increases the complexity and computational overhead in the system which increases the processing time. To mitigate the drawbacks of fuzzy logic systems, hybrid approaches combining fuzzy logic with other deep learning techniques can be used [26, 40, 78, 79]. This is the reason, we have combined deep learning based models to fuzzy logic and which has enhanced the system performance. The output of the fuzzy logic system is typically a set of membership values or degrees of confidence associated with different diagnostic categories. These filtered values will help us to accurately identify diseases.The use of fuzzy membership functions provides a layer of rule-based interpretability, allowing clinicians to trace how pixel intensities contribute to a specific diagnostic category, which serves as a pre-requisite for full XAI integration.

Strength, Weakness and Extensions

The study demonstrates the author's expertise in medical image analysis by utilizing advanced segmentation designs such as U-Net, Pruned U-Net, Attention U-Net, and U-Net++. These models, combined with fuzzy logic, effectively address the ambiguity and vagueness inherent in medical imaging data, thereby enhancing the accuracy and reliability of diagnoses. The integration of augmentation techniques within the Fuzzy Dilated CNN model further promotes generalizability and adaptability, which are crucial for diverse clinical settings.

However, the study is limited to X-ray images and focuses on specific respiratory conditions, including Bacterial Pneumonia, Tuberculosis, COVID-19, Viral Pneumonia, and normal cases. This specialization may restrict the applicability of the findings to other types of medical imaging modalities or different pathological conditions. Additionally, the research only explores common optimizers like Adam, leaving other optimizers such as Gradient Descent unexplored [80, 81]. Furthermore, the study does not address the impact of these technological advances on clinical practice or their usefulness in patient care, which are essential considerations for translating technical breakthroughs into real-world healthcare success.

Future extensions of this research should include broader application domains and direct translation studies that consider clinical decision-making and patient care. One potential area of study is the effect of different X-ray scanners on AI systems [82], as seen in previous research on automatic computer-based tracings in longitudinal 2-D ultrasound images using various scanners. Additionally, designing risk assessment systems for immunology applications [83], like those developed for coronary artery disease risk assessment in intravascular ultrasound, could be beneficial. Converting the system into a screening and classification tool for different types of pneumonia, as exemplified by automatic vessel identification for angiographic screening [84], is another valuable direction. Additionally, the use of transformers in the model architecture has shown potential for further enhancing performance in medical image analysis [85]. Lastly, discussions on bias, such as those in the context of an AI framework for brain tumor segmentation, are essential to ensure the ethical and unbiased application of these technologies in medical settings [21, 86].While this study demonstrates the quantitative 'Fuzzy Effect' on accuracy, future work will include Grad-CAM and heatmaps to visually validate the alignment between fuzzy-enhanced features and clinical lung pathologies.Ensemble methods [88, 89] have the potential to further improve performance on this dataset; we plan to evaluate and report on these approaches in future work.

8. Conclusion

Our study presents a comprehensive analysis of various segmentation and classification models applied to medical image analysis, focusing on chest X-ray images. Firstly, our investigation into four segmentation performance across Bacterial Pneumonia, Tuberculosis, COVID-19, Viral Pneumonia, and Normal cases, reveals notable outcomes. Attention U-Net consistently emerges as a top performer, with better accuracy, Jaccard index, and Dice coefficient compared to U-Net, Pruned U-Net, and U-Net++. Moreover, our exploration into the impact of augmentation techniques on classification tasks highlights substantial improvements in model performance. Augmentation enhances the robustness and adaptability of the Fuzzy Dilated CNN model, particularly evident in classes like Bacterial Pneumonia, Tuberculosis, and Normal cases. The augmentation not only improves precision, recall, and F1-scores but also enhances the AUC values, indicating better discriminative ability and overall model effectiveness. In conclusion, our findings emphasize the critical role of attention mechanisms and augmentation techniques in advancing medical image analysis. By leveraging attention U-Net segmentation and augmentation with Fuzzy Dilated CNN, we have demonstrated significant improvements in segmentation and classification tasks, ultimately contributing to more accurate and reliable diagnostic predictions. These insights are instrumental in shaping the future of medical imaging technology, with the potential to revolutionize healthcare delivery and improve patient outcomes on a global scale.

Ethics Statement

This study did not involve direct human or animal participation, and all analyses were conducted using anonymized chest X-ray datasets (Available on Request). Therefore, ethical approval and informed consent were not required. The research was carried out in accordance with relevant guidelines and regulations for the use of open-access medical imaging data.

Data Availability: The data supporting the findings of this study can be found at following link: COVID-19 Radiography Database. Available online: `https://www.kaggle.com/tawsifurrahman/covid19-radiography-database`, Tuberculosis (TB) Chest X-ray Database. Available online: `https://www.kaggle.com/tawsifurrahman/tuberculosis-tb-chest-xray-dataset`, Kaggle's Chest X-ray Images (Pneumonia) Dataset. 2020. Available online: `https://www.kaggle.com/paultimothymooney/chest-xray-pneumonia`

Funding: The authors declare that no funds, grants, or other financial support were received during the preparation of this manuscript.

Conflict of Interest: The authors declare that they have no relevant financial or non-financial interests to disclose.

References

[1] A. El-Baz and J. S. Suri, *Lung imaging and computer aided diagnosis*. CRC Press, 2011.

[2] R. Shashidhara, N. Ahuja, M. Lajuvanthi, S. Akhila, A. K. Das, and J. J. Rodrigues, "SDN-chain: Privacy-preserving protocol for software defined networks using blockchain," *Security and Privacy*, vol. 4, no. 6, p. e178, 2021.

[3] R. Cau et al., "Complications in COVID-19 patients: Characteristics of pulmonary embolism," *Clinical Imaging*, vol. 77, pp. 244-249, 2021.

[4] J. S. Suri et al., "COVID-19 pathways for brain and heart injury in comorbidity patients: A role of medical imaging and artificial intelligence-based COVID severity classification: A review," *Computers in biology and medicine*, vol. 124, p. 103960, 2020.

[5] N. Sharma, L. Saba, N. N. Khanna, M. K. Kalra, M. M. Fouda, and J. S. Suri, "Segmentation-based classification deep learning model embedded with explainable AI for COVID-19 detection in chest X-ray scans," *Diagnostics*, vol. 12, no. 9, p. 2132, 2022.

[6] S. Sharma and K. Guleria, "A systematic literature review on deep learning approaches for pneumonia detection using chest X-ray images," *Multimedia Tools Applications*, pp. 1-51, 2023.

[7] M. S. Ahmed et al., "Joint Diagnosis of Pneumonia, COVID-19, and Tuberculosis from Chest X-ray Images: A Deep Learning Approach," *Diagnostics*, vol. 13, no. 15, p. 2562, 2023.

[8] S. Sharma and K. Guleria, "A Deep Learning based model for the Detection of Pneumonia from Chest X-Ray Images using VGG-16 and Neural Networks," *Procedia Computer Science*, vol. 218, pp. 357-366, 2023.

[9] L. Pervizaj-Oruqaj et al., "Alveolar macrophage-expressed Plet1 is a driver of lung epithelial repair after viral pneumonia," *Nature Communications*, vol. 15, no. 1, p. 87, 2024.

[10] Y. Liao et al., "Interleukin-18-primed human umbilical cord-mesenchymal stem cells achieve superior therapeutic efficacy for severe viral pneumonia via enhancing T-cell immunosuppression," *Cell Death Disease*, vol. 14, no. 1, p. 66, 2023.

[11] M. N. Islam et al., "Interpretable Differential Diagnosis of Non-COVID Viral Pneumonia, Lung Opacity and COVID-19 Using Tuned Transfer Learning and Explainable AI," in *Healthcare*, 2023, vol. 11, no. 3: MDPI, p. 410.

[12] T. Sahu et al., "Infection and potential challenge of childhood mortality in sickle cell disease: a comprehensive review of the literature from a global perspective," *Thalassemia Reports*, vol. 13, no. 3, pp. 206-229, 2023.

[13] A. Watson and T. M. Wilkinson, "Respiratory viral infections in the elderly," *Therapeutic advances in respiratory disease*, vol. 15, p. 1753466621995050, 2021.

[14] G. Fekadu et al., "Impact of COVID-19 pandemic on chronic diseases care follow-up and current perspectives in low resource settings: a narrative review," *International journal of physiology, pathophysiology and pharmacology*, vol. 13, no. 3, p. 86, 2021.

[15] K. E. Mason, G. Maudsley, P. McHale, A. Pennington, J. Day, and B. Barr, "Age-adjusted associations between comorbidity and outcomes of COVID-19: a review of the evidence from the early stages of the pandemic," *Frontiers in Public Health*, vol. 9, p. 584182, 2021.

[16] K. Siddiqi, B. Stubbs, Y. Lin, H. Elsey, and N. Siddiqi, "TB multimorbidity: a global health challenge demanding urgent attention," *The International Journal of Tuberculosis and Lung Disease*, vol. 25, no. 2, pp. 87-90, 2021.

[17] J. Ferreira-Coimbra, C. Sarda, and J. Rello, "Burden of community-acquired pneumonia and unmet clinical needs," *Advances in therapy*, vol. 37, no. 4, pp. 1302-1318, 2020.

[18] N. N. Khanna et al., "Vascular implications of COVID-19: role of radiological imaging, artificial intelligence, and tissue characterization: a special report," *Journal of cardiovascular development and disease*, vol. 9, no. 8, p. 268, 2022.

[19] M. Biswas et al., "State-of-the-art review on deep learning in medical imaging," *Frontiers in Bioscience-Landmark*, vol. 24, no. 3, pp. 380-406, 2019.

[20] J. S. Suri et al., "Deep learning paradigm for cardiovascular disease/stroke risk stratification in Parkinson's disease affected by COVID-19: a narrative review," *Diagnostics*, vol. 12, no. 7, p. 1543, 2022.

[21] S. Agarwal et al., "COVLIAS 3.0: cloud-based quantized hybrid UNet3+ deep learning for COVID-19 lesion detection in lung computed tomography," *Frontiers in Artificial Intelligence*, vol. 7, p. 1304483, 2024.

[22] H. A. Zaki et al., "The Battle of the Pneumonia Predictors: A Comprehensive Meta-Analysis Comparing the Pneumonia Severity Index (PSI) and the CURB-65 Score in Predicting Mortality and the Need for ICU Support," *Cureus*, vol. 15, no. 7, 2023.

[23] A. Cobat, Q. Zhang, C. H. G. Effort, L. Abel, J.-L. Casanova, and J. Fellay, "Human genomics of COVID-19 pneumonia: Contributions of rare and common variants," *Annual Review of Biomedical Data Science*, vol. 6, pp. 465-486, 2023.

[24] S. Ehrmann et al., "Inhaled amikacin to prevent ventilator-associated pneumonia," *New England Journal of Medicine*, vol. 389, no. 22, pp. 2052-2062, 2023.

[25] S. Goyal and R. Singh, "Detection and classification of lung diseases for pneumonia and Covid-19 using machine and deep learning techniques," *Journal of Ambient Intelligence Humanized Computing*, vol. 14, no. 4, pp. 3239-3259, 2023.

[26] P. K. Jain, N. Sharma, A. A. Giannopoulos, L. Saba, A. Nicolaides, and J. S. Suri, "Hybrid deep learning segmentation models for atherosclerotic plaque in internal carotid artery B-mode ultrasound," *Computers in biology and medicine*, vol. 136, p. 104721, 2021.

[27] V. K. Shrivastava, N. D. Londhe, R. S. Sonawane, and J. S. Suri, "A novel and robust Bayesian approach for segmentation of psoriasis lesions and its risk stratification," *Computer methods and programs in biomedicine*, vol. 150, pp. 9-22, 2017.

[28] S. Das, G. K. Nayak, L. Saba, M. Kalra, J. S. Suri, and S. Saxena, "An artificial intelligence framework and its bias for brain tumor segmentation: A narrative review," *Computers in biology and medicine*, vol. 143, p. 105273, 2022.

[29] A. K. Dubey et al., "Ensemble deep learning derived from transfer learning for classification of COVID-19 patients on hybrid deep-learning-based lung segmentation: a data augmentation and balancing framework," *Diagnostics*, vol. 13, no. 11, p. 1954, 2023.

[30] J. Wu et al., "Medsegdiff: Medical image segmentation with diffusion probabilistic model," in *Medical Imaging with Deep Learning*, 2024: PMLR, pp. 1623-1639.

[31] S. Priyadarsini, K. Pushpadevi, and S. Chitra, "Medical image segmentation using UNet algorithm," in *AIP Conference Proceedings*, 2024, vol. 2802, no. 1: AIP Publishing.

[32] L. Mohanty, A. Kumar, V. Mehta, M. Agarwal, and J. S. Suri, "Pruning techniques for artificial intelligence networks: a deeper look at their engineering design and bias: the first review of its kind," *Multimedia Tools and Applications*, pp. 1-75, 2024.

[33] N. Das and S. Das, "Attention-UNet architectures with pretrained backbones for multi-class cardiac MR image segmentation," *Current Problems in Cardiology*, vol. 49, no. 1, p. 102129, 2024.

[34] S. Metlek, "CellSegUNet: an improved deep segmentation model for the cell segmentation based on UNet++ and residual UNet models," *Neural Computing Applications*, pp. 1-27, 2024.

[35] J. S. Suri et al., "UNet deep learning architecture for segmentation of vascular and non-vascular images: a microscopic look at UNet components buffered with pruning, explainable artificial intelligence, and bias," *Ieee Access*, vol. 11, pp. 595-645, 2022.

[36] P. K. Jain et al., "Attention-based UNet deep learning model for plaque segmentation in carotid ultrasound for stroke risk stratification: an artificial intelligence paradigm," *Journal of Cardiovascular Development and Disease*, vol. 9, no. 10, p. 326, 2022.

[37] J. S. Suri et al., "COVLIAS 1.0 lesion vs. medseg: An artificial intelligence framework for automated lesion segmentation in COVID-19 lung computed tomography scans," *Diagnostics*, vol. 12, no. 5, p. 1283, 2022.

[38] L. d. F. Costa, "Further generalizations of the Jaccard index," *arXiv preprint arXiv:2110.09619*, 2021.

[39] L. R. Dice, "Measures of the amount of ecologic association between species," *Ecology*, vol. 26, no. 3, pp. 297-302, 1945.

[40] S. S. Skandha et al., "A hybrid deep learning paradigm for carotid plaque tissue characterization and its validation in multicenter cohorts using a supercomputer framework," *Computers in biology and medicine*, vol. 141, p. 105131, 2022.

[41] S. K. Gupta, "3-D optimized classification and characterization artificial intelligence paradigm for cardiovascular/stroke risk stratification using carotid ultrasound-based delineated plaque: Atheromatic™ 2.0," 2020.

[42] A. El-Baz and J. S. Suri, *Lung Cancer and Imaging*. IOP Publishing, 2019.

[43] G. D. Rubin et al., "The role of chest imaging in patient management during the COVID-19 pandemic: a multinational consensus statement from the Fleischner Society," *Radiology*, vol. 296, no. 1, pp. 172-180, 2020.

[44] W. Ahmad and U. Ahmad, "Role of radiology in COVID-19 pandemic and post COVID-19 potential effects on radiology practices," *Indian Journal of Radiology and Imaging*, vol. 31, no. S 01, pp. S196-S197, 2021.

[45] J. J. Cavallo and H. P. Forman, "The economic impact of the COVID-19 pandemic on radiology practices," *Radiology*, vol. 296, no. 3, pp. E141-E144, 2020.

[46] G. Pujolar, A. Oliver-Anglès, I. Vargas, and M.-L. Vázquez, "Changes in access to health services during the COVID-19 pandemic: a scoping review," *International journal of environmental research and public health*, vol. 19, no. 3, p. 1749, 2022.

[47] H. Zacher and C. W. Rudolph, "Individual differences and changes in subjective wellbeing during the early stages of the COVID-19 pandemic," *American Psychologist*, vol. 76, no. 1, p. 50, 2021.

[48] R. Najjar, "Redefining radiology: a review of artificial intelligence integration in medical imaging," *Diagnostics*, vol. 13, no. 17, p. 2760, 2023.

[49] A. Barragán-Montero et al., "Artificial intelligence and machine learning for medical imaging: A technology review," *Physica Medica*, vol. 83, pp. 242-256, 2021.

[50] L. J. Ewals et al., "The Effects of Artificial Intelligence Assistance on the Radiologists' Assessment of Lung Nodules on CT Scans: A Systematic Review," *Journal of Clinical Medicine*, vol. 12, no. 10, p. 3536, 2023.

[51] X. Tang, "The role of artificial intelligence in medical imaging research," *BJR— Open*, vol. 2, no. 1, p. 20190031, 2019.

[52] J. Potočnik, S. Foley, and E. Thomas, "Current and potential applications of artificial intelligence in medical imaging practice: A narrative review," *Journal of Medical Imaging and Radiation Sciences*, 2023.

[53] M. Agarwal et al., "A novel block imaging technique using nine artificial intelligence models for COVID-19 disease classification, characterization and severity measurement in lung computed tomography scans on an Italian cohort," *Journal of Medical Systems*, vol. 45, no. 3, p. 28, 2021.

[54] L. Saba et al., "Six artificial intelligence paradigms for tissue characterisation and classification of non-COVID-19 pneumonia against COVID-19 pneumonia in computed tomography lungs," *International journal of computer assisted radiology and surgery*, vol. 16, pp. 423-434, 2021.

[55] L. Jones, D. Golan, S. Hanna, and M. Ramachandran, "Artificial intelligence, machine learning and the evolution of healthcare: A bright future or cause for concern?," *Bone & joint research*, vol. 7, no. 3, pp. 223-225, 2018.

[56] A. Lin, M. Kolossváry, I. Išgum, P. Maurovich-Horvat, P. J. Slomka, and D. Dey, "Artificial intelligence: improving the efficiency of cardiovascular imaging," *Expert review of medical devices*, vol. 17, no. 6, pp. 565-577, 2020.

[57] B. Acs, M. Rantalainen, and J. Hartman, "Artificial intelligence as the next step towards precision pathology," *Journal of internal medicine*, vol. 288, no. 1, pp. 62-81, 2020.

[58] S. M. Lee et al., "Deep learning applications in chest radiography and computed tomography: current state of the art," *Journal of thoracic imaging*, vol. 34, no. 2, pp. 75-85, 2019.

[59] F. Molinari, L. Gaetano, G. Balestra, and J. S. Suri, "Role of fuzzy pre-classifier for high performance LI/MA segmentation in B-mode longitudinal carotid ultrasound images," in *2010 Annual International Conference of the IEEE Engineering in Medicine and Biology*, 2010: IEEE, pp. 4719-4722.

[60] U. R. Acharya, N. Kannathal, E. Ng, L. C. Min, and J. S. Suri, "Computer-based classification of eye diseases," in *2006 International Conference of the IEEE Engineering in Medicine and Biology Society*, 2006: IEEE, pp. 6121-6124.

[61] Q. Jiang, J. Huang, X. Jin, P. Wang, W. Zhou, and S. Yao, "Medical image fusion using a new entropy measure between intuitionistic fuzzy sets joint Gaussian curvature filter," *IEEE Transactions on Radiation Plasma Medical Sciences*, vol. 7, no. 5, pp. 494-508, 2023.

[62] V. Narayan, P. K. Mall, S. Awasthi, S. Srivastava, and A. Gupta, "FuzzyNet: Medical image classification based on GLCM texture feature," in *2023 International Conference on Artificial Intelligence and Smart Communication (AISC)*, 2023: IEEE, pp. 769-773.

[63] X. Zhao and W. Xu, "NFMPAtt-Unet: Neighborhood fuzzy c-means multi-scale pyramid hybrid attention unet for medical image segmentation," *Neural Networks*, vol. 178, p. 106489, 2024.

[64] C. Wang, X. Lv, M. Shao, Y. Qian, and Y. Zhang, "A novel fuzzy hierarchical fusion attention convolution neural network for medical image super-resolution reconstruction," *Information Sciences*, vol. 622, pp. 424-436, 2023.

[65] B. Ragupathy and M. Karunakaran, "A fuzzy logic-based meningioma tumor detection in magnetic resonance brain images using CANFIS and U-Net CNN classification," *International Journal of Imaging Systems Technology*, vol. 31, no. 1, pp. 379-390, 2021.

[66] P. Sanga et al., "DermAI 1.0: A robust, generalized, and novel attention-enabled ensemble-based transfer learning paradigm for multiclass classification of skin lesion images," *Diagnostics*, vol. 13, no. 19, p. 3159, 2023.

[67] A. Mumuni and F. Mumuni, "Data augmentation: A comprehensive survey of modern approaches," *Array*, vol. 16, p. 100258, 2022.

[68] E. E. Kerre and M. Nachtegael, *Fuzzy techniques in image processing*. Physica, 2013.

[69] P. K. Jain, N. Sharma, M. K. Kalra, A. Johri, L. Saba, and J. S. Suri, "Far wall plaque segmentation and area measurement in common and internal carotid artery ultrasound using U-series architectures: An unseen Artificial Intelligence paradigm for stroke risk assessment," *Computers in Biology and Medicine*, vol. 149, p. 106017, 2022.

[70] D. Keidar et al., "COVID-19 classification of X-ray images using deep neural networks," *European radiology*, vol. 31, no. 12, pp. 9654-9663, 2021.

[71] Y. Peng, Y. Tang, S. Lee, Y. Zhu, R. M. Summers, and Z. Lu, "COVID-19-CT-CXR: a freely accessible and weakly labeled chest X-ray and CT image collection on COVID-19 from biomedical literature," *IEEE transactions on big data*, vol. 7, no. 1, pp. 3-12, 2020.

[72] Y. Wang et al., "Prediction of viral pneumonia based on machine learning models analyzing pulmonary inflammation index scores," *Computers in Biology Medicine*, vol. 169, p. 107905, 2024.

[73] H. Abdulah et al., "CXR-Net: an artificial intelligence pipeline for quick COVID-19 screening of chest X-rays," *arXiv preprint arXiv:.00087*, vol. 87, 2021.

[74] E. Ayan, B. Karabulut, and H. M. Ünver, "Diagnosis of pediatric pneumonia with ensemble of deep convolutional neural networks in chest x-ray images," *Arabian Journal for Science Engineering*, pp. 1-17, 2022.

[75] D. Singh et al., "Fuzzy logic based medical diagnostic system for hepatitis B using machine learning," *Soft Computing*, pp. 1-17, 2023.

[76] L. A. Zadeh, "Fuzzy sets," *Information and control*, vol. 8, no. 3, pp. 338-353, 1965.

[77] J. M. Mendel, "Uncertain rule-based fuzzy systems," *Introduction and new directions*, vol. 684, 2017.

[78] M. Kaur, "Large-scale bound constrained optimization based on hybrid teaching learning optimization algorithm," 2021.

[79] J. S. Suri et al., "Inter-variability study of COVLIAS 1.0: hybrid deep learning models for COVID-19 lung segmentation in computed tomography," *Diagnostics*, vol. 11, no. 11, p. 2025, 2021.

[80] R. Cau et al., "Cine-cardiac magnetic resonance to distinguish between ischemic and non-ischemic cardiomyopathies: a machine learning approach," *European Radiology*, pp. 1-14, 2024.

[81] R. Cau et al., "Base-to-apex Gradient Pattern Assessed by Cardiovascular Magnetic Resonance in Takotsubo Cardiomyopathy," *Journal of Thoracic Imaging*, vol. 39, no. 4, pp. 217-223, 2024.

[82] F. Molinari, W. Liboni, P. Giustetto, S. Badalamenti, and J. S. Suri, "Automatic computer-based tracings (ACT) in longitudinal 2-D ultrasound images using different scanners," *Journal of Mechanics in Medicine and Biology*, vol. 9, no. 04, pp. 481-505, 2009.

[83] T. Araki et al., "PCA-based polling strategy in machine learning framework for coronary artery disease risk assessment in intravascular ultrasound: A link between carotid and coronary grayscale plaque morphology," *Computer methods and programs in biomedicine*, vol. 128, pp. 137-158, 2016.

[84] K. Liu and J. S. Suri, "Automatic vessel indentification for angiographic screening," ed: Google Patents, 2005.

[85] S. Gupta et al., "Four Transformer-Based Deep Learning Classifiers Embedded with an Attention U-Net-Based Lung Segmenter and Layer-Wise Relevance Propagation-Based Heatmaps for COVID-19 X-ray Scans," *Diagnostics*, vol. 14, no. 14, p. 1534, 2024.

[86] P. K. Rao, S. Chatterjee, and S. Sharma, "Weight pruning-UNet: Weight pruning UNet with depth-wise separable convolutions for semantic segmentation of kidney tumors," *Journal of Medical Signals & Sensors*, vol. 12, no. 2, pp. 108-113, 2022.

[87] Nillmani, P.; Jain, P.K.; Sharma, N.; Kalra, M.K.; Viskovic, K.; Saba, L.; Suri, J.S. Four Types of Multiclass Frameworks for Pneumonia Classification and Its Validation in X-ray Scans Using Seven Types of Deep Learning Artificial Intelligence Models. Diagnostics 2022, 12, 652.https://doi.org/10.3390/diagnostics12030652

[88] Mamun, M., Chowdhury, S. H., Hossain, M. M., Khatun, M. R., & Iqbal, S. (2025). Explainability enhanced liver disease diagnosis technique using tree selection and stacking ensemble-based random forest model. Informatics and Health, 2(1), 17-40.

[89] Hussain MI, Munir A, Mamun M, Chowdhury SH, Uddin N, Hossain MM. A Transparent House Price Prediction Framework Using Ensemble Learning, Genetic Algorithm-Based Tuning, and ANOVA-Based Feature Analysis. FinTech. 2025; 4(3):33. https://doi.org/10.3390/fintech4030033